Appl. Phys. A (2016) 122:415
DOI 10.1007/s00339-016-9863-7

Applied Physics A
Materials Science & Processing

INVITED PAPER

Metal hydride hydrogen compression: recent advances and future prospects

Volodymyr A. Yartys[1,2] · Mykhaylo Lototskyy[3] · Vladimir Linkov[3] · David Grant[4] · Alastair Stuart[4] · Jon Eriksen[5] · Roman Denys[5] · Robert C. Bowman Jr.[6]

Received: 29 September 2015 / Accepted: 14 November 2015 / Published online: 17 March 2016

Abstract Metal hydride (MH) thermal sorption compression is one of the more important applications of the MHs. The present paper reviews recent advances in the field based on the analysis of the fundamental principles of this technology. The performances when boosting hydrogen pressure, along with two- and three-step compression units, are analyzed. The paper includes also a theoretical modelling of a two-stage compressor aimed at describing the performance of the experimentally studied systems, their optimization and design of more advanced MH compressors. Business developments in the field are reviewed for the Norwegian company HYSTORSYS AS and the South African Institute for Advanced Materials Chemistry. Finally, future prospects are outlined presenting the role of the MH compression in the overall development of the hydrogen-driven energy systems. The work is based on the analysis of the development of the technology in Europe, USA and South Africa.

1 Introduction

The present work is aimed at review of the recent progress made in the past years, particularly in the framework of the International Energy Agency Task 32 Hydrogen Based Energy Storage, in the area of the thermally driven systems for storage and compression of hydrogen gas utilizing metal hydrides (MHs).

Metal hydride (MH) hydrogen compression utilizes a reversible heat-driven interaction of a hydride-forming metal, alloy or intermetallic compound with hydrogen gas to form MH and is considered as a promising application for hydrogen energy systems. This technology, which initially arose in early 1970s, still offers a very good alternative to both conventional (mechanical) and newly developed (electrochemical, ionic liquid pistons) methods of hydrogen compression. The advantages of MH compression include simplicity in design and operation,

✉ Volodymyr A. Yartys
volodymyr.yartys@ife.no

Mykhaylo Lototskyy
mlototskyy@uwc.ac.za

Vladimir Linkov
vlinkov@uwc.ac.za

David Grant
David.Grant@nottingham.ac.uk

Alastair Stuart
Alastair.Stuart@nottingham.ac.uk

Jon Eriksen
jon.eriksen@hystorsys.no

Roman Denys
roman.denys@hystorsys.no

Robert C. Bowman Jr.
rcbjr1967@gmail.com

[1] Institute for Energy Technology, P.O. Box 40, 2027 Kjeller, Norway

[2] Norwegian University of Science and Technology, 7491 Trondheim, Norway

[3] South African Institute for Advanced Materials Chemistry, University of the Western Cape, Robert Sobukwe Road, Private Bag X17, Bellville 7535, South Africa

[4] Faculty of Engineering, University of Nottingham, Nottingham NG7 2RD, UK

[5] HYSTORSYS AS, P.O. Box 45, 2027 Kjeller, Norway

[6] Oak Ridge National Laboratory, P.O. Box 2008, Oak Ridge, TN 37831, USA

absence of moving parts, compactness, safety and reliability, and the possibility to utilize waste industrial heat instead of locally generated or purchased electricity for much, if not all, of the heating of the MH containers.

The use of the waste industrial heat is a major winning argument for MH compression by allowing dramatic decreases in operational costs.

A state-of-the-art review on MH hydrogen compression technology was recently published by Lototskyy et al. [1]. The studies reported after publishing this review were mainly focused on the development and characterization of MH materials for hydrogen compression [2–5], modelling of the MH compression systems [6, 7], components and system developments [7–10], including a review by Bhuiya et al. [10] on non-hydrogen storage MH applications. Other applications for MH compressors described since Ref. [1] was published include generating high pressure for in situ powder XRD studies [11] and MH-driven actuators [12].

This article outlines the critical components of the MH hydrogen compression technology with a focus on the phase equilibria in the metal–hydrogen systems and modelling of the heat and mass transfer processes in the coupled MH beds. The authors also present some recent developments of industrial-scale MH hydrogen compressors at HYSTORSYS AS/Norway and SAIAMC/UWC/South Africa. Finally, we briefly describe some additional recently proposed applications for the MH hydrogen compression technology.

1.1 General concept of the MH compression

Metal hydride hydrogen compression uses a reversible heat-driven interaction of a hydride-forming metal/alloy, or intermetallic compound with hydrogen gas, to form a MH:

$$\mathrm{M(s)} + x/2\,\mathrm{H_2(g)} \underset{\text{desorption}}{\overset{\text{absorption}}{\rightleftharpoons}} \mathrm{MH}_x\mathrm{(s)} + Q; \qquad (1)$$

where M denotes the hydride-forming metal/alloy/intermetallic compound, (s) and (g) relate to the solid and gas phases, respectively. The direct forward process results in an exothermic formation of the MH hydrogen absorption and is accompanied by the release of heat, Q, equal to the absolute value of the hydrogenation enthalpy, $|\Delta H|$. The reverse process results in endothermic hydride decomposition/hydrogen desorption, requiring supply of approximately the same amount of heat at a higher operating temperature.

Equilibrium of the reaction (1) is characterized by an interrelation between hydrogen pressure (P), concentration of hydrogen in the solid (C) and temperature (T). This relation (PCT diagram) is the characteristic feature of a specific hydride-forming material determining thermodynamics of its interaction with gaseous hydrogen.

At low hydrogen concentrations ($0 \le C < a$), hydrogen atoms form an interstitial solid solution in the metal matrix (α-phase) with $C(H) \sim \sqrt{P(H_2)}$ according to Henry–Sieverts law. When the value of C exceeds concentration of the saturated solid solution (a), a precipitation of the hydride (β-phase with hydrogen concentration $b > a$) nucleates, and the system ideally behaves according to the first-order phase transition law taking place at a constant hydrogen pressure, $P = P_P$ ($a \le C \le b$). This pressure is identified as a plateau pressure in the diagrams of the metal–hydrogen systems. A further increase in hydrogen concentration is again accompanied by the pressure increase corresponding to the formation of an H solid solution in the β-phase. When the concentration approaches a certain maximum value ($C \to C_{max}$) corresponding to the maximum hydrogen capacity of the material (i.e., the number of hydrogen atoms filling all interstitial sites available for the insertion of H atoms), the equilibrium pressure exhibits an asymptotic increase, $P \to \infty$.

The plateau width, (b–a), is often considered as a reversible hydrogen capacity of the material, and the equilibrium of reaction (1) in the plateau region is described by a van't Hoff equation:

$$\ln\left(\frac{P_P}{P^0}\right) = -\frac{\Delta S^0}{R} + \frac{\Delta H^0}{RT}; \qquad (2)$$

where $P^0 = 1$ atm. $= 1.013$ bar, ΔS^0 and ΔH^0 are the standard entropy and enthalpy of hydride formation, respectively, and R is the universal gas constant.

Since the plateau pressure, P_P, increases exponentially with the temperature (see Fig. 1), the low-temperature

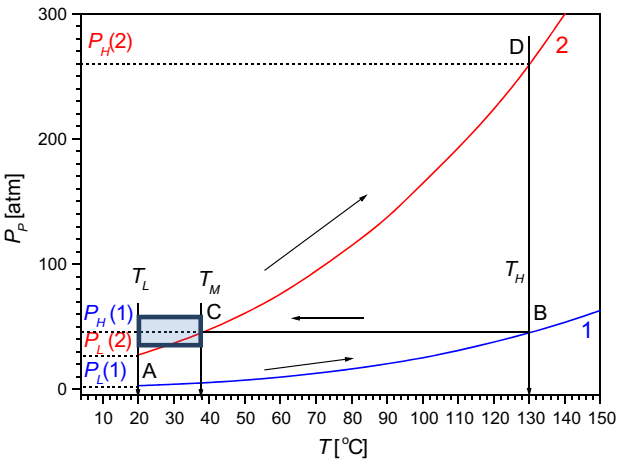

Fig. 1 Temperature dependence of plateau pressure, P_P, for the systems of gaseous H_2 with $La_{0.85}Ce_{0.15}Ni_5$ (1) and C14-$Ti_{0.65}Zr_{0.35}$(-Mn,Cr,Fe,Ni)$_2$ (2). Both dependencies are presented for H desorption at H concentration in the solid equal to 75 NL/kg that corresponds to H/AB$_5$ = 2.90 and H/AB$_2$ = 1.15. The *rectangular area* corresponds to pressures and temperatures during H_2 absorption in stage 2 in the course of two-stage operation

($T = T_L$) H absorption at $P_{H2} > P_P(T_L) = P_L$ takes place at a lower hydrogen pressure and the high-temperature ($T = T_H$) H desorption ($P_{H2} < P_P(T_H) = P_H$) occurs at a higher pressure, similar to the suction and discharge processes in a mechanical compressor.

Figure 1 illustrates a general concept of the MH hydrogen compression realized with the use of intermetallic alloys $La_{0.85}Ce_{0.15}Ni_5$ (1) and C14-$Ti_{0.65}Zr_{0.35}$(Mn,Cr,Fe,Ni)$_2$ (2) applied by IFE and SAIAMC/UWC in their developments of the thermally driven MH hydrogen compressors. At $T_L = 20$ °C, the hydrogenated alloys have plateau pressures of $P_L(1) = 3.5$ atm. and $P_L(2) = 20$ atm., respectively, while at $T_H = 130$ °C, the plateau pressures are $P_H(1) = 45.5$ atm. and $P_H(2) = 261$ atm., yielding the compression ratios of about 13 in both cases.

In contrast, by application of a two-stage operation it is possible to achieve H_2 compression from $P_L(1) = 3.5$ atm. to $P_H(2) = 261$ atm. (compression ratio 74.6) in the same temperature range. In such a process, the medium-pressure hydrogen at $P_L(2) \le P_M \le P_H(1)$ is desorbed from the AB_5-type hydride (1) at the temperature $T = T_H$ (process AB) and further absorbed in the AB_2-type alloy (2) at $T_L \le T \le T_M$ (process BC) followed by the desorption at $T = T_H$ and $P = P_H$ (2; process CD).

The dependencies 1 and 2 shown in Fig. 1 were built on the basis of the experimental PCT data for both alloys further processed by modelling [13] with an average calculation error in H concentrations below 2 NL/kg. At the same time, they still represent idealized performance of the MH compressor, without taking into account hysteresis and cycle productivity.

More precise thermodynamic estimations can be done by considering the whole hydrogen absorption and desorption isotherms (Fig. 2). The isotherms for $La_{0.85}Ce_{0.15}Ni_5$ (stage 1) and C14-$Ti_{0.65}Zr_{0.35}$(Mn,Cr,Fe,Ni)$_2$ (stage 2) were also built using the model [13] with the parameters obtained by the refinement of the experimental PCT data.

As shown in Fig. 2, the two-stage hydrogen compression from $P_L = 10$ bar to $P_H = 200$ bar (overall compression ratio 20) in temperature range from $T_L = 20$ °C to $T_H = 130$ °C involves the following processes:

- AB: Hydrogen absorption in the stage 1 MH material at P_L and T_L;
- BC: Hydrogen desorption from the stage 1 MH at $T = T_H$ and an intermediate pressure, P_M;
- CD: Hydrogen absorption in the stage 2 MH at P_M and T_L;
- DEF: Hydrogen desorption from the stage 2 MH at T_H and P_H.

Each process is accompanied by the transfer of hydrogen, and the overall process cycle productivity will be determined by the minimum amount of the transferred hydrogen

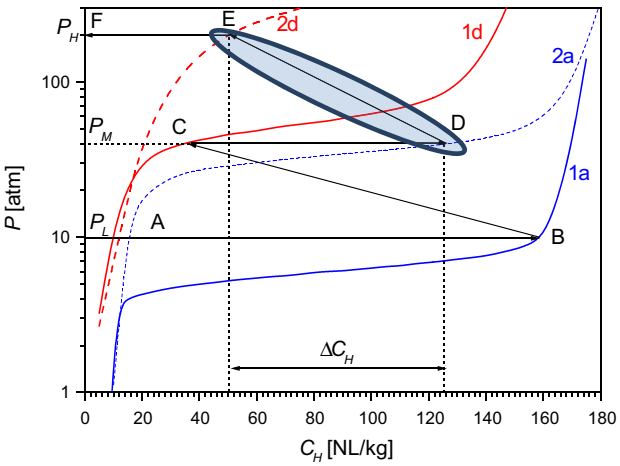

Fig. 2 Isotherms of hydrogen absorption at $T_L = 20$ °C (*a*) and desorption at $T_H = 130$ °C (*d*) for the systems of gaseous H_2 with $La_{0.85}Ce_{0.15}Ni_5$ (1) and C14-$Ti_{0.65}Zr_{0.35}$(Mn,Cr,Fe,Ni)$_2$ (2). The *circled area* corresponds to the minimum amount of the transferred hydrogen (ΔC_H) in the course of two-stage H_2 compression process ABCDEF

(ΔC_H) in the course of two-stage H_2 compression process ABCDEF. As shown in Fig. 2, this minimum amount (process DE; $\Delta C_H = 75$ NL/kg at $P_M = 40$ atm.), as a rule, is determined by under-saturation of the stage 2 material during H_2 transfer between the first and the second stage of the MH compressor (process CD). This feature was observed experimentally in [14] in the course of the tests of 10–200 bar MH hydrogen compressor at SAIAMC/UWC which utilized the same hydride materials for the stages 1 and 2.

In summary, accurate thermodynamic estimation of hydrogen compression performance of MH materials, including process cycle productivity (ΔC_H) at the given suction (P_L) and discharge (P_H) pressures and cooling (T_L) and heating (T_H) temperatures is especially critical for the multistage H_2 compression and becomes possible when complete isotherms of hydrogen absorption at T_L and hydrogen desorption at T_H, accounting for plateau slope and hysteresis, are taken into consideration. This assessment can be done by the fitting the available experimental PCT data using suitable models of phase equilibria in metal–hydrogen systems. We note that the model also has to take into account the features of H–M phase diagram since in wide range of the operating temperatures ($T_L \ldots T_H$) a noticeable change of the concentrations (*a*, *b*) limiting the two-phase ($\alpha + \beta$) concentration region of the pressure–composition isotherms is observed (see Fig. 2).

During the developments of thermally driven MH hydrogen compressors at IFE, HYSTORSYS AS and SAIAMC/UWC, the authors (VY, ML, VL) mainly used the model [13] which takes these features into account by assuming H atoms in the solid as a Van der Waals lattice

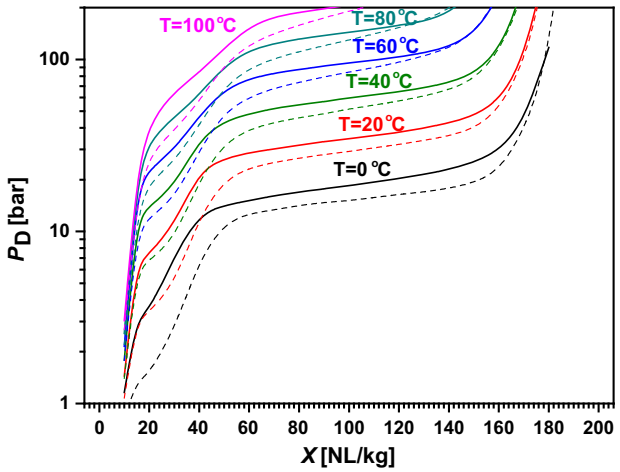

Fig. 3 Calculated PCT diagram for H absorption (*solid lines*) and desorption (*dashed lines*) in the mixture 90 wt% C14-$(Ti,Zr)(Mn,Cr,Fe,Ni)_2$ + 10 wt% $La_{0.8}Ce_{0.2}Ni_5$

gas and Gaussian distribution of the plateau pressures. In addition, the model uses Kierstead's approach [15] in order to simulate pressure–composition isotherms when there are several plateau segments. The latter feature is very useful for the estimation of hydrogen compression performances of the "multiplateau" systems, both for some intermetallics (e.g., TiFe) and also for the mixtures of different MH materials.

Figure 3 presents calculated PCT diagram of MH material on the basis of C14-$Ti_{0.65}Zr_{0.35}(Mn,Cr,Fe,Ni)_2$ used for H_2 compression to 200 bar and higher at the heating temperatures below 130–150 °C. The material also contains 10 wt% $La_{0.8}Ce_{0.2}Ni_5$ added for the improvement of the activation performances of the AB_2-type intermetallic. The fitting parameters of the model [13] obtained by the refinement of the separately taken PCT data for the AB_2- and AB_5-type alloys allowed us to reconstruct the PCT diagram of the mixture that, in turn, improved accuracy of modelling the performances of the corresponding compression elements.

2 Proof of concept: a single-step 350 L/200 bar MH hydrogen storage and compression unit using AB_5-type alloy

The first developments of MH units combining hydrogen storage and compression occurred in the late 1960s during the pioneer work by Wiswall and Reilly [16]. Similar solutions were developed in the Russian Federal Nuclear Centre (VNIIEF), disclosed in late 1990s [17]. The latter are rather impressive: Vanadium hydride was heated to ~500 °C [17] generating hydrogen pressures as high as 5 kbar. A significant contribution to the art was also done in 1980–1990s by the group from Institute of Mechanical Engineering Problems/Academy of Science of Ukraine (IPMach; see [18]). One of the important features of these developments was in the original engineering solution allowing to control the output hydrogen pressure by introducing a feedback between its value and the heating/cooling power supplied to the MH bed.

All the solutions provide hydrogen storage in MH and its periodic supply at higher pressure to a consumer. Since the main attention here was mainly paid to the system layout, without optimization of the MH material for the application, the units had low productivities and efficiencies and, as a rule, were characterized by too high temperatures necessary to provide the required output pressure. For example, the mentioned developments by IPMach, where $LaNi_5H_x$ was mainly used, required temperatures 250–300 °C to reach the output pressures 100–150 bar. Also, in the time when the developments were implemented, the lack of digital electronics did not allow to completely realize all the advantages of the proposed engineering solutions, especially those ones which concerned the automated pressure control.

We consider the small-scale (~100 NL H_2) units for hydrogen storage and compression as convenient facilities for the testing of MH materials for hydrogen compression at the conditions maximally close to ones for the application. Moreover, such units can be used as efficient laboratory equipment providing safe and simple in operation supply of high-pressure hydrogen gas to experimental facilities.

This development has arisen more recently as a result of activities of hydrogen storage group at the Institute for Energy Technology, Department of Energy Systems. These activities are devoted to the implementation of MHs for high-pressure hydrogen compression and were started in 2003. Some preliminary results, including the development of the experimental prototype of 200 NL/160 bar H storage and compression unit (with the participation of the Institute for Problems of Materials Science, National Academy of Science of Ukraine), were published [19]. Finally, the 350 NL/200 bar unit being described in this section uses an AB_5 hydrogen storage alloy in combination with electric heating and air cooling. This has been built and experimentally studied, to specify dependencies between generated pressure and MH bed temperature, as well as to estimate the discharge dynamic performances. Also, an important result was in the creation of the supply system providing our experimental facilities with hydrogen at high pressure, with the possibility to precisely set its value.

AB_5 alloys, where A is rare earth metal and B is mainly nickel, are the most frequently used materials for MH applications. Their main advantages are low sensitivity to poisoning by impurities, easy activation and fast H

sorption–desorption kinetics. The broad range of PCT versatility and tunability is evident for AB_5, with the room-temperature plateau pressure variable over three orders of magnitude depending on the composition [20]. On the other hand, many AB_5 alloys are subject to degradation via disproportionation reactions during extended cycling to elevated temperatures as described in Ref. [1]. It is also known that substitution of Al or Sn for a portion of the Ni results in greatly enhanced stabilities, while heating treatments at low pressure and temperatures circa 400 °C produce nearly 100 % recovery of the hydrogen storage performances [1].

Figure 4a shows our estimations of the formation enthalpies of intermetallic hydrides $La_{1-x}Ce_xNi_5H_y$ based on the available reference data [21]. The corresponding calculation of hydrogen equilibrium pressures (Fig. 4b) assuming $\Delta S^0 = -110$ J/(mole H_2 K) shows that at the composition of the intermetallic corresponding to the formula $La_{0.85}Ce_{0.15}Ni_5$ the pressures above 200 bar can be generated at the temperatures below 180 °C, and at room temperature the equilibrium pressure is below 10 bar. It satisfies our primary objective as to pressure–temperature ranges for MH hydrogen compression. At the same time, the cerium contents in the alloy is low enough that allows to avoid such negative features of Ce-rich intermetallics as lower H storage capacity and increased hysteresis.

The alloy of the specified composition $La_{0.85}Ce_{0.15}Ni_5$ which is indicated by dashed line in Fig. 4 was purchased from Labtech Int. Co. Ltd., supplied in the powdered form.

According to XRD analysis of different batches of the starting and hydrogenated[1] alloy from various suppliers, both comprised the $CaCu_5$-type single or major[2] phase with lattice periods varying within $a = 4.99$–5.02 Å, $c = 3.995$–3.999 Å for the parent intermetallic and volume increase upon hydrogenation, $\Delta V/V_0$, between 24 and 24.5 %.

Figure 5 shows PCT diagram of hydrogen absorption and desorption by the $La_{0.85}Ce_{0.15}Ni_5$ H storage alloy. The experimental data (points) were fitted using our model of phase equilibria in metal–hydrogen systems [13]; the calculated PCT diagram is presented as the wire-frame surface. The modelling/fitting procedure also used the equilibrium data obtained during the tests of the unit containing the same H storage alloy. For simplicity, we did not take into account hysteresis, using both absorption and desorption data. According preliminary PCT studies, the

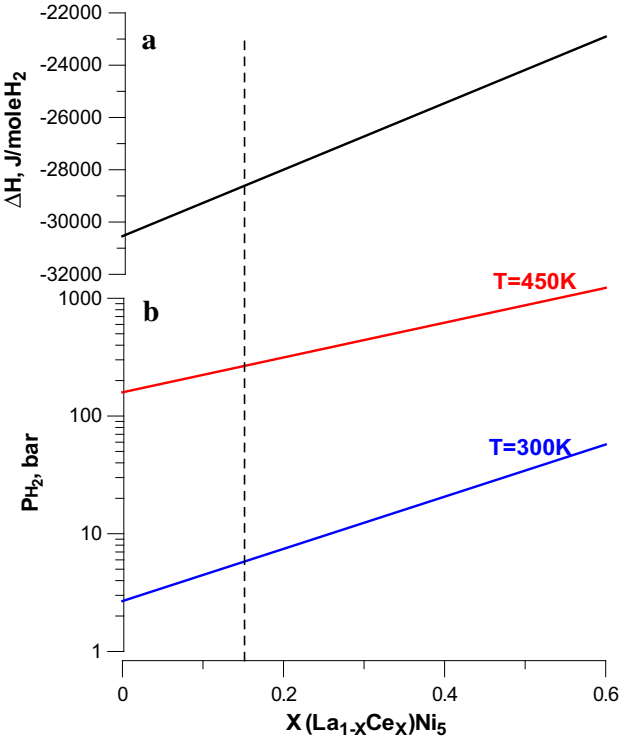

Fig. 4 Estimated enthalpies of hydride formation for cerium-substituted intermetallic $LaNi_5$ (*a*) and the corresponding values of equilibrium hydrogen pressure at different temperatures (*b*) calculated assuming the entropy of the hydride formation equal to −110 J/(mole H_2 K)

hysteresis energy losses, $RT \ln\left(P_A/P_D\right)$, were less than 900 J/mole H_2 that corresponds to $\left(P_A/P_D\right) \approx 1.4$ at room temperature, or $\left(\frac{T_A - T_D}{T_D}\right) < 0.04$. We think that these differences are not so significant for our case, since other uncertainties (e.g., introduced by temperature distribution in the MH bed) can result in a bigger contribution to the observed PCT data.

The calculated pressure–temperature dependencies for H_2 desorption from the hydrogenated $La_{0.85}Ce_{0.15}Ni_5$ are shown in Fig. 6. It is seen that at the higher saturations of the alloy with hydrogen (>60 % of the maximum hydrogen storage capacity) rather high pressures (>150 bar) can be generated by the heating of the material to the temperatures up to 200 °C.

The data presented in Figs. 5 and 6 confirm our estimations (Fig. 4): The plateau pressure at rather low temperature of 150 °C exceeds 100 bar, and at ambient temperature ($T = 30$ °C), it is between 10 and 20 bar that is acceptable for the application. The maximum hydrogen sorption capacity approaches 6.0 H/AB_5 corresponding to 155 NL/kg. The reversible H storage capacity, as shown in Fig. 5, is more than 90 % of the corresponding maximum

[1] Before taking XRD of the hydrogenated samples, the hydrides were stabilized by the exposition on air at $T = 77$ K; the patterns showed the presence of two phases including intermetallic hydride with increased unit cell volume, and α-solid solution with the lattice periods close to those of the starting alloy.

[2] In some samples, impurity of Ni (<0.5 wt%) was observed.

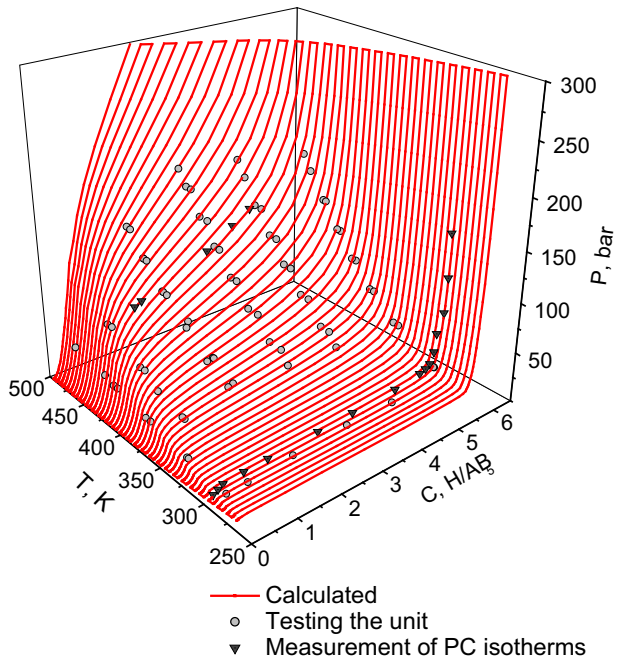

Fig. 5 Calculated PCT diagram of the H storage alloy (*wire-frame surface*) obtained by the fitting of the experimental pressure–composition isotherms (*shaded inverse triangles*) and the experimental PCT data taken in the course of testing the unit (*circles*)

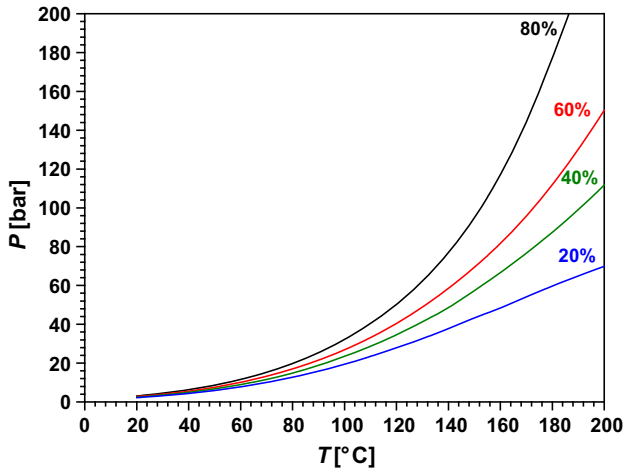

Fig. 6 Calculated temperature dependencies of H desorption equilibrium pressure for the system H_2–$La_{0.85}Ce_{0.15}Ni_5$ at different hydrogen concentrations; the values in percentage of the maximum hydrogen capacity (155 NL/kg) are shown as *curve labels*

value. Both absorption and desorption of hydrogen at the experimental conditions were fast: more than 90 % of hydrogen is absorbed/desorbed in <10–15 min.

A general view and schematics of the hydrogen storage and supply system are presented in Fig. 7. The MH container (1) is fixed to the perforated horizontal shelf of a cabinet where the whole system (gas communications and electronics) is assembled. The shut-off diaphragm valves (2) installed on the front panel of the cabinet provide manually operated connection of the container's gas manifold with H_2 discharge or charge lines whose ports (5 and 6, respectively) are installed on the rear panel. For overpressure protection, the gas manifold is also connected with a port of venting line (7), via relief valve (3) adjusted to a cracking pressure of 210 bar. The gas manifold of the container (1) is also connected to a 210-bar pressure sensor (4; Omega PX482A-3KSI, 4–20 mADC output). All the connections are performed using ¼″ OD stainless steel tubing and the corresponding Swagelok tube fittings.

Hydrogen supply at higher pressures is provided by heating the MH bed in the container (1), by cartridge electric heater (1a; 230 VAC, 800 W) axially placed in the container. Heat dissipation is provided by external air cooling with two fans (12; 230 VAC, 28 W each) placed under the perforated shelf.

A simplified control diagram of the system is presented in Fig. 7d. The main output of the control circuit is the electric power supplied to the heater (1a) of the MH container (1). The control circuit has two inputs, viz. the temperature in the container measured by the thermocouple (1b; K-type) and the hydrogen pressure measured by the pressure sensor (4; Omega PX482A-3KSI). The last parameter provides the main feedback signal (DC current proportional to hydrogen pressure) monitored by the display unit (10; Omega DP24-E-230) and simultaneously connected to the input of the PID controller (8; Eurotherm 2408). The output of the controller (8) is connected to the input of a power amplifier (11; TF10a) via on/off controller (9; Eurotherm 2132) whose input is connected to the thermocouple (1b). The output of the power amplifier (11) is connected to the heater (1a). In turn, the auxiliary on/off output (alarm relay) of the PID controller (8) provides switching cooling fans (12) on and off.

During the operation, the PID controller (8), together with the power amplifier (11), provides power supply to the heater (1a) of the MH container (1). Heating the MH container stimulates hydrogen desorption from the MH at a higher pressure which is monitored by the sensor (4). When the pressure approaches the setpoint of the PID controller (8), it reduces the power supplied to the heater (1a), similarly to its standard operation in temperature control mode. If pressure overshoot takes place, the alarm relay of the PID controller (8) switches the fans (12) on, resulting in the cooling of the MH container and corresponding decrease in the hydrogen pressure.

The setpoint of the controller (9) all the time is equal to maximum allowed temperature of the MH container (200 °C). When the temperature monitored by the thermocouple (1b) reaches this value (it occurs at the end of discharge where hydrogen equilibrium pressures above

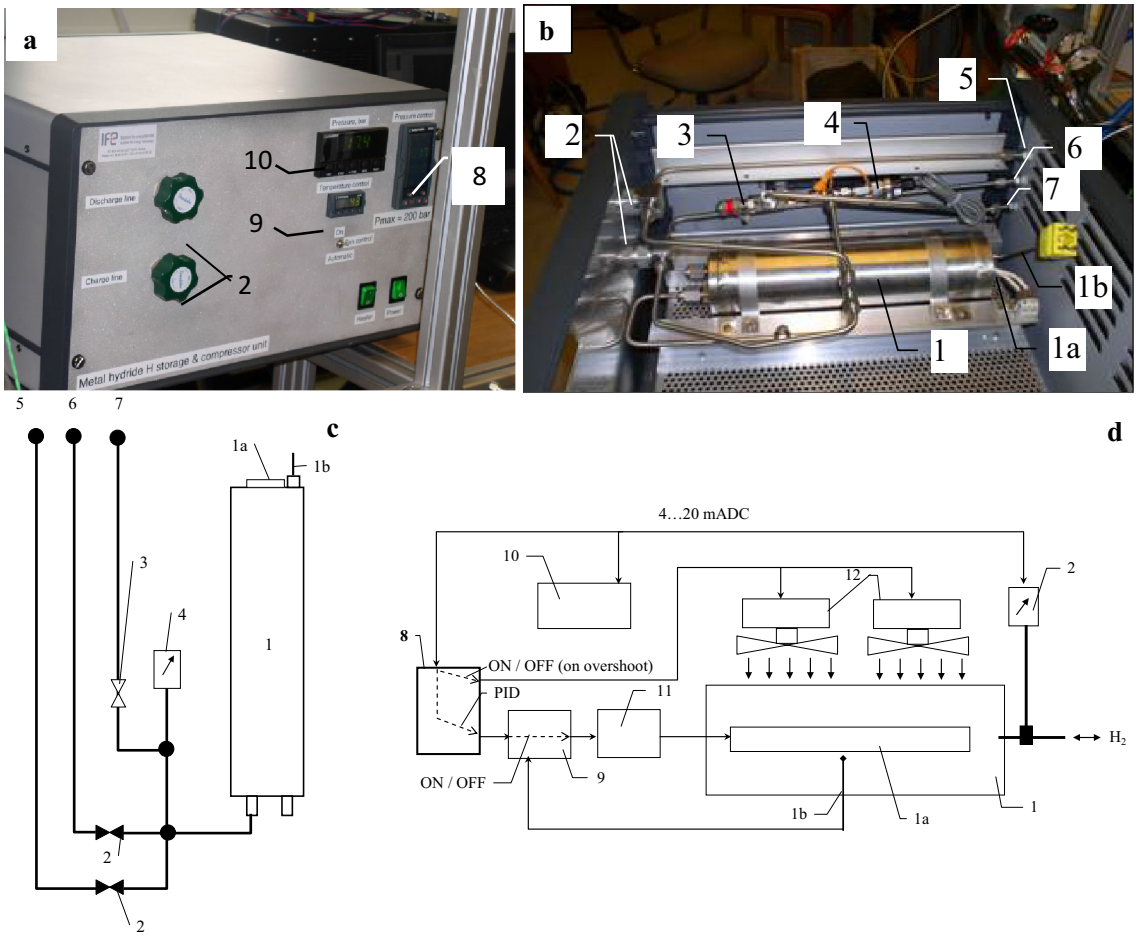

Fig. 7 Control diagram (**a**), general overview (**b**), gas communications (**c**) and control diagram (**d**) of 350 NL/200 bar MH hydrogen storage and compression unit. *1*—MH container (*1a*—cartridge electric heater, *1b*—thermocouple), *2*—shut-off valves, *3*—safety relief valve, *4*—pressure sensor, *5*—H_2 discharge line, *6*—H_2 charge line, *7*—venting line, *8*—pressure controller, *9*—auxiliary temperature controller/indicator, *10*—pressure indicator, *11*—power amplifier and *12*—fans

depleted MH can be reached only at higher temperatures), power supply to the heater (1a) is switched off, and the heating is resumed when the temperature decreases below 200 °C.

Figure 8 presents assembly drawing of the MH container used in the system. The powdered MH bed is placed in the space formed by stainless steel bottom flange (1), external tubular shell (2), top flange (3) and the internal heat exchanger (4). The latter is formed by the stainless steel core tube (outer diameter 25.4 mm, wall thickness 2.64 mm) and aluminum 1060 fins (height 15.8 mm, thickness 0.4 mm, pitch 2.3 mm). The inner space (1a) of the heat exchanger (4) is adjusted for the tight fit of the cartridge-type electric heater. To reduce thermally induced stresses, only one end of core tube of the heat exchanger is fixed rigidly (welded) to the flange (1); the other end is plugged and left in the non-fixed position. The top flange (3) of the container is equipped with the male VCR-type metal gasket face seal fittings for input/output of hydrogen

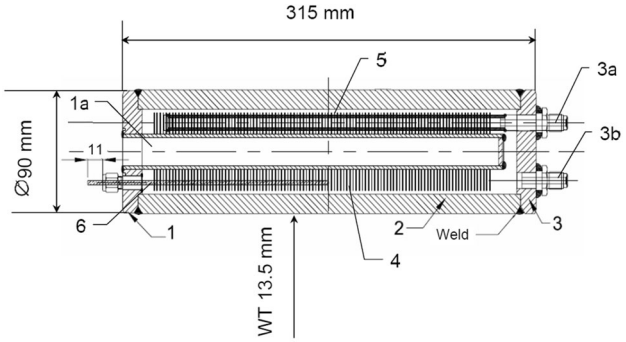

Fig. 8 Assembly drawing of the MH container. *1*—bottom SS flange (*1a*—space for electric heater), *2*—shell (SS tube), *3*—top flange (*3a*—H2 input/output, *3b*—MH loading), *4*—heat exchanger (SS tube/Al fins), *5*—filter (porous SS tube) and *6*—thermocouple

gas (3a) and loading/unloading the MH powder (3b). The gas fitting (3a) is connected with the tubular porous stainless steel filter (5), pore size of 5 μ. The top flange (1)

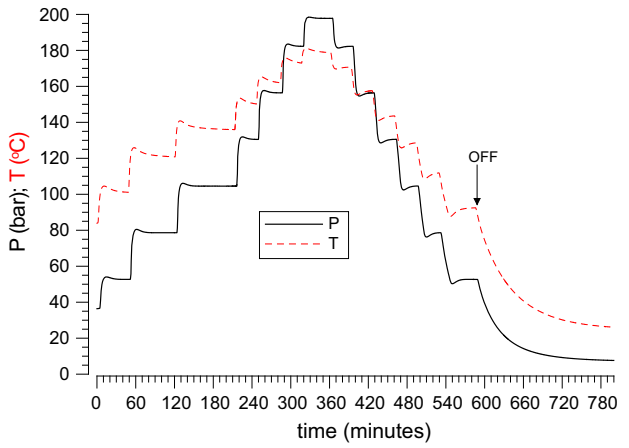

Fig. 9 Cyclogram of the operation of the MH H storage and compression unit. The starting residual amount of stored hydrogen is equal to 182 NL (83 NL/kg, $H/AB_5 = 3.15$)

of the container has the fitting where stainless steel shield of the K-type thermocouple (6) is firmly fixed. The junction of the thermocouple (6) is located in the middle of the MH bed, with respect to both its length and thickness.

The design of the MH container (Fig. 8) allows its prolonged operation at gas pressures up to 200 bar and temperatures up to 200 °C. In addition, after its assembly the container has successfully passed the test at gas pressure (argon) up to 300 bar and temperature up to 250 °C; test duration at the most extreme conditions (300 bar/250 °C) was about 10 min. The test was performed by RAUFOSS Fuel Systems ASA, with the participation of the authors (ML, VY; test report RAFS-00205, May 12, 2006).

The internal volume of the MH container is 640 cm^3 that corresponds to the total amount of the H_2 storage alloy of 2.234 kg, at the filling density of 3.5 g/cm^3, or ~53 % of the density of the hydrogenated alloy, in accordance with the upper limit of safe packing fraction (<61 %) for AB_5-type hydrides reported in the literature [22]. At the same time, such an amount of the alloy provides the specified H_2 storage capacity of 350 NL H_2.

Under testing conditions, the setpoint after its increase was reached in 10 min, and in 20 min the pressure stabilization mode was established. The maximum overshoot did not exceed 5 bar. After decreasing the setpoint, it was reached in 15 min, and the time of pressure stabilization was about 30 min. Both the reproducibility of the pressure setpoint and stability of its maintaining were better than 0.05 %. As shown in Fig. 9, generation of hydrogen pressure in the range 50–200 bar requires moderate temperatures, 100–180 °C.

The maximum output flow rate determined in the course of discharge of the unit to the medium-pressure Sieverts' setup (total discharge volume about 3 l) was about 10 NL/min (Fig. 10). At $H/AB_5 > 2.5$ and $P < 40$ bar, the rate of

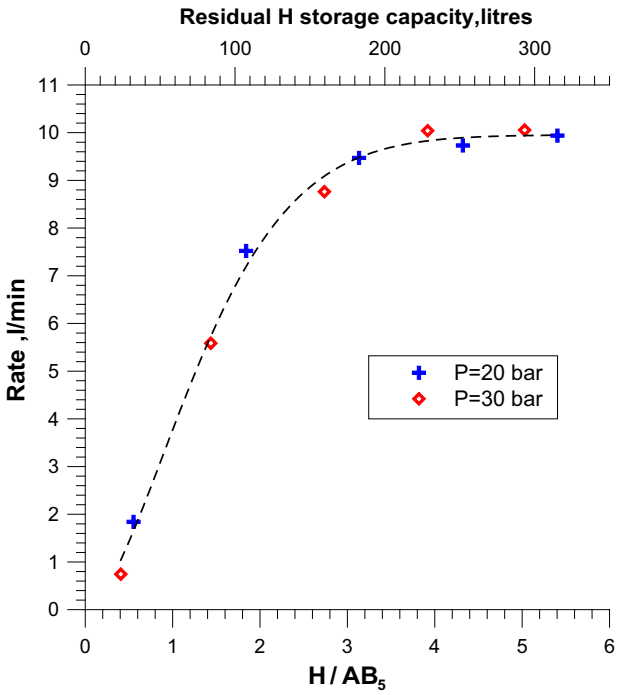

Fig. 10 Dependence of the unit's discharge flow rate on the residual hydrogen concentration in MH. Points correspond to the measurements done in the course of different discharges of the unit to the total receiver volume ~3 l, at pressure setpoint equal to 50 bar. *Dashed line* is plotted just to guide the eye

the discharge does not significantly depend on pressure or on hydrogen concentration in MH; while at lower H concentration the discharge rate is proportional to it.

In our opinion based on the application of the analysis of performances of MH compressors [1] to the present development, the main contribution to the limitation of the discharge dynamics is introduced by a too high heat capacity of the empty MH container whose weight (~10 kg) exceeds the weight of the MH material by more than four times. It is also confirmed by the slow dynamics of charging the unit, as well as by its slow cooling/decreasing pressure, after turning the unit off (see the last descending segment of the *P–T* curves in Fig. 9). To radically improve the dynamic performances of high-pressure MH TSC, it is necessary to find the novel engineering solutions of its main component part, MH container, which should combine the high enough mechanical strength with minimal heat capacity, i.e., minimal material consumption and weight.

Results of testing of the MH hydrogen storage and compression unit have confirmed our supposition that such an apparatus can be very efficient and convenient in operation laboratory equipment providing experimental facilities with hydrogen supplied at predefined higher pressures. To reveal its potential on the market of laboratory equipment, we finally made a brief economic analysis based on real costs for the used standard components, as

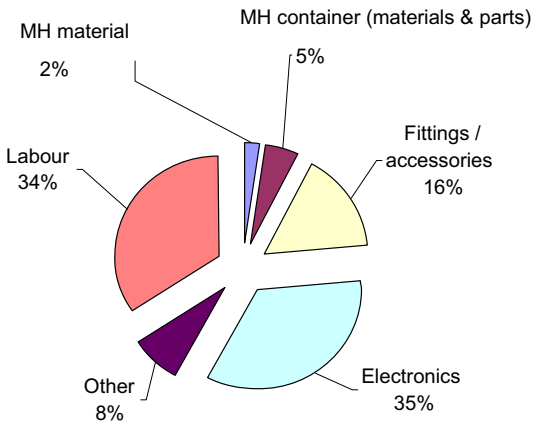

Fig. 11 Cost structure of the MH H storage and compression unit. The estimated labor costs correspond to 0.5 man-month total workload

well as on the estimations of workload/labor costs necessary for the production of the unit.

The total manufacture costs are estimated at 43–45 thousand Norwegian crowns (NOK) that is the same order as the price of ordinary laboratory equipment, such as thermostats, vacuum systems.

The main categories of the costs are shown in Fig. 11. In contrast to other applications of MH, the presented one is characterized by rather low fraction of MH material in the total cost, 2 % against 15–50 % for MH hydrogen storage units [23]. It does mean that for the selection of MH material for this application good kinetics and durability performances should be main criteria, and it is not so critical to optimize its cost. The most expensive categories ($\sim$35 % each) are electronics and labor. Both, especially the latter, are subjects for the optimization, by optimizing system layout and nonstandard components (first of all, MH container) and improving their making technology.

In summary, the developed unit was shown to allow an efficient control of the output hydrogen pressure that can be used in various applications including safe and simple in operation supply of laboratory facilities with high-pressure hydrogen gas.

The feasibility to generate up to 200 bar H_2 pressure by a MH compressor using AB_5 H storage alloys and temperatures <200 °C was shown as well.

3 Modelling a two-step MH compressor: simulation of a domestic refueller

Unlike petrol and diesel, hydrogen can easily be generated on-site and therefore the energy can be distributed by electrons via the electricity grid, or where there is a local renewable energy source, zero-carbon hydrogen can be generated. The developments in both passenger and commercial hydrogen vehicles are making it more attractive for end users to generate their own hydrogen to service either a single vehicle (much like the attraction of plug-in hybrids) or a small fleet of vehicles (this could either be a community facility for domestic use or for a commercial fleet). The domestic refueller concept is based on the premise that the average car owner drives less than 40 miles per day which equates to ca. 600 g of H_2. Based on a multistage MH compressor system and 1.5 kW electrolyzer, the domestic refueller would be capable of providing an overnight top-up of an H_2 FCEV in preparation for the following days commute at a target pressure of 350 bar.

3.1 Numerical simulation

The successful operation of a multistage MH compressor system introduces strict requirements into the tunability of the pressure–composition isotherm (PCI) characteristics. The plateau pressure for the hydrogenation process of the first-stage material should be sufficiently low in order for the material to be able to absorb the hydrogen from the low pressure supplied by the electrolyzer. The coupling of the first stage (dehydrogenation) and the second stage (hydrogenation) requires the plateau pressure (p_{eq}) of the stage 1 MH to be higher than that of stage 2 MH. The higher the pressure differential between stages 1 and 2 plateau pressures, the greater the force that delivers the transfer of hydrogen from the first stage to second stage of the tanks and drives the second-stage hydrogenation. In order to achieve a sufficiently high compression ratio to meet the target of 350 bar delivery pressure, the plateau pressure of the dehydrogenation process for the second-stage material should be as high as possible. Figure 12 illustrates the two-stage compression cycle on a van't Hoff plot, where it is assumed that stage 1 and stage 2 hydride beds share the same temperature range of low temperature, T_L, up to a high temperature T_H. The compression cycle process is summarized as follows: Step A: A low-pressure hydrogen supply (e.g., an electrolyzer) is attached to the first stage, at pressure P_s. The temperature of stage 1 is maintained at T_L, during hydrogenation. Step B–C: A sensible heating process for the stage 1 MH bed occurs, heating the bed to T_H and increasing the pressure of the stage 1 vessel. Step D–E: A coupling process between stage 1 (dehydrogenation at T_H) and stage 2 (hydrogenation at T_L) occurs. Step F–G: Stage 2 hydride bed undergoes sensible heating in order to achieve the delivery pressure of P_d. Step H: During dehydrogenation of stage 2 high-pressure hydrogen is released from the compressor at P_d.

The additional complexity in the design of this application that two coupled MH reactors introduce warrants the use of a numerical model [7] in order to predict the overall compressor performance. Once validated, a numerical

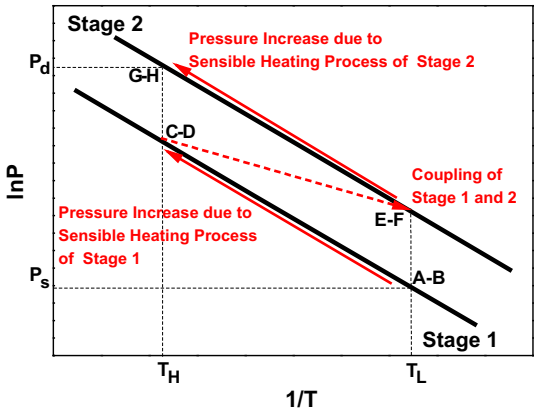

Fig. 12 A van't Hoff plot illustrating the operation of a two-stage metal hydride hydrogen compression system from the low temperature T_L to the high temperature T_H. A sensible heating process is performed after each hydrogenation process to increase P_{eq} inside each compression stage. For clarity, the *black lines* represent the van't Hoff plot for the hydrogenation process for stage 1 (*lower black line*) and for stage 2 (*upper black line*).The coupling process between stage 1 and stage 2 is represented by the *dashed line*

model will allow the timely optimization of specific system parameters and the incorporation of enhanced heat management techniques leading to the improvement of overall compressor performance.

3.2 Assumptions

The following assumptions are made simplifying the MH compression operation for purposes of this analysis:

(a) Initially, the MH bed temperature and pressure profiles are uniform.
(b) Thermal conductivity and specific heat of the MH's are assumed constant during the compression cycle.
(c) The MH and hydrogen gas are in local thermal equilibrium which implies that there is no heat transfer between solid and gas phases.
(d) The hydrogen gas can be treated as an ideal gas from a thermodynamic point of view.

3.3 Heat equation

Assumption (c), thermal equilibrium between the hydride powder and hydrogen gas, allows the numerical model to be implemented by solving a single heat equation in place of separate equations for the solid and gas phases:

$$(\rho \cdot Cp)_e \cdot \frac{\partial T}{\partial t} + (\rho_g \cdot Cp_g) \cdot \bar{v}_g \cdot \nabla T = \nabla \cdot (k_e \cdot \nabla T) + m \cdot \left(\left(\frac{\Delta H}{M_{H_2}} \right) - T \cdot (Cp_g - Cp_s) \right) \quad (3)$$

where the effective heat capacity is given by:

$$(\rho \cdot Cp)_e = \varepsilon \cdot \rho_g \cdot C_{pg} + (1 - \varepsilon) \cdot \rho_s \cdot C_{ps} \quad (4)$$

and the effective thermal conductivity is given by:

$$k_e = \varepsilon \cdot k_g + (1 - \varepsilon) \cdot k_s \quad (5)$$

The terms ρ_g, C_{pg}, C_{ps} and m refer to the density of the gas phase, the heat capacity of the gas phase, the heat capacity of the solid phase and the kinetic term for the reaction, respectively.

3.4 Hydrogen mass balance

The equation that describes the diffusion of hydrogen mass inside the metal matrix is:

$$\varepsilon \frac{\partial(\rho_g)}{\partial t} + \mathrm{div}(\rho_g \vec{v}_g) = \pm m \quad (6)$$

where $(-)$ is for the hydrogenation process and $(+)$ is for the dehydrogenation process, v_g is the velocity of gas during diffusion within the metal lattice (see Sect. 3.5 below), and m is the mass of hydrogen diffused per unit time and unit volume in the metal lattice.

3.5 Momentum equation

The velocity of a gas passing through a porous medium can be expressed by Darcy's law. By neglecting the gravitational effect, the equation which gives the velocity of gas inside the metal matrix is given by:

$$\vec{v}_g = -\frac{K}{\mu_g} \cdot \mathrm{grad}(\vec{P}_g) \quad (7)$$

where K is the permeability of the solid and μ_g is the dynamic viscosity of gas.

3.6 Kinetic expression

The amount of hydrogen taken up by the hydride bed during hydrogenation is given by:

$$m_a = C_a \cdot \exp\left[-\frac{E_a}{R_g \cdot T} \right] \cdot \ln\left[\frac{\rho_g}{P_{eq}} \right] \cdot (\rho_{ss} - \rho_s) \quad (8)$$

The amount of hydrogen released from the hydride bed during dehydrogenation is given by:

$$m_d = C_d \cdot \exp\left[-\frac{E_d}{R_g \cdot T} \right] \cdot \left(\frac{P_{eq} - \rho_g}{P_{eq}} \right) \cdot \rho_s \quad (9)$$

where ρ_s and ρ_{ss} are the density of the hydride at any time and at saturation state, respectively. C_{abs} and C_{des} refer to the pre-exponential constants, and the E_a and E_d are the activation energy for hydrogenation and dehydrogenation processes, respectively.

3.7 Equilibrium pressure

In order to incorporate the effect of hysteresis and the plateau slope (which is present in both stages of the compression cycle) into the calculation of the plateau pressure P_{eq}, the following equation was used [24, 25]

$$\ln P_{eq} = \left[\frac{\Delta H}{RT} - \frac{\Delta S}{R} + (\varphi_s \pm \varphi_0)\right] \cdot \times \tan\left[\pi \cdot \left(\frac{x}{x_{sat}} - \frac{1}{2}\right) \pm \frac{\beta}{2}\right] \times 10^5 \quad (10)$$

where φ_s and φ_0 describe the plateau flatness factors and β is the factor which can describe the hysteresis ($\ln P_{abs}/P_{des}$). Furthermore, "+" refers for the hydrogenation process, while "−" refers for the dehydrogenation process and x and x_{sat} are the hydrogen concentration at any given time and fully saturated.

3.8 Mass and energy balance during multistage reactor coupling

During the coupling between the two reactors (stage 1—dehydrogenation process and stage 2—hydrogenation process), the total number of the hydrogen moles in the space of the connector between stages 1 and 2 at any time is given by:

$$n_{t+dt} = n_t + n_{des} - n_{abs} \quad (11)$$

where n_t and n_{t+dt} are, respectively, the number of hydrogen moles in the total space at any time t and $t + dt$. The number of the moles of hydrogen released from the stage 1 during the dehydrogenation process is n_{des} and the number of hydrogen moles stored in stage 2 in a small time dt is n_{abs}. At any time the gas pressure in the connecting pipe between the two rectors, which is the driving force for both the hydrogenation and dehydrogenation process, is calculated by:

$$P_{t+dt} = \frac{n_{t+dt} \cdot R \cdot T_{t+dt}}{V_{des} + V_{abs}} \quad (12)$$

where T_{t+dt} is the temperature of gas in the connecting pipe, V_{des} and V_{abs} are the free volume of the reactors during the dehydrogenation process (V_{des}) and the hydrogenation process (V_{abs}). The pressure in the connecting pipe acts as the driving force for both the dehydrogenation and the hydrogenation process, so for the coupling case the kinetics for the dehydrogenation and the hydrogenation are calculated by:

$$m_{des} = C_{des} \exp\left[-\frac{E_{des}}{RT}\right] \cdot \frac{\vec{P}_{eq} - P_{t+dt}}{P_{eq}} \cdot \rho_s \quad (13)$$

$$m_{abs} = C_{abs} \exp\left[-\frac{E_{abs}}{RT}\right] \cdot \ln\left(\frac{P_{t+dt}}{P_{eq}}\right) \cdot \Delta\rho_s \quad (14)$$

Validation of the numerical model was achieved through comparing the model with the experimental work given in [7].

3.9 Simulation results and analysis

A numerical simulation was conducted using COMSOL Multiphysics version 4.3b, a finite element-based numerical solver. The initial temperature of the first-stage hydrogenation process and dehydrogenation processes was 20 and 130 °C, respectively, and the properties of the first-stage material were those of an AB_5 ($La_{0.85}Ce_{0.15}Ni_5$) alloy, while the properties of the second-stage material were based on an AB_2 (Zr–V–Mn) alloy. The initial pressure for the stage was 15 bar, representing the pressure that a commercial electrolyzer can provide. Figure 13 shows the average bed temperature for the two-stage compression system. A complete two-stage compression cycle consists of one non-coupled hydrogenation process (stage 1), one coupled dehydrogenation (stage 1)–hydrogenation (stage 2) process, a dehydrogenation process (stage 2) and two sensible heating processes (stages 1 and 2). For clarity, the two sensible heating processes have not been shown, but are represented in Figs. 13 and 14 by the vertical dashed line at the end of the first-stage hydrogenation process, the coupling and the beginning of the dehydrogenation process. After the hydrogenation process of stage 1, sensible heating takes place raising the temperature inside the reactor from 20 to 130 °C. Figure 14 shows the bed average pressure evolution of the compression system. Initially,

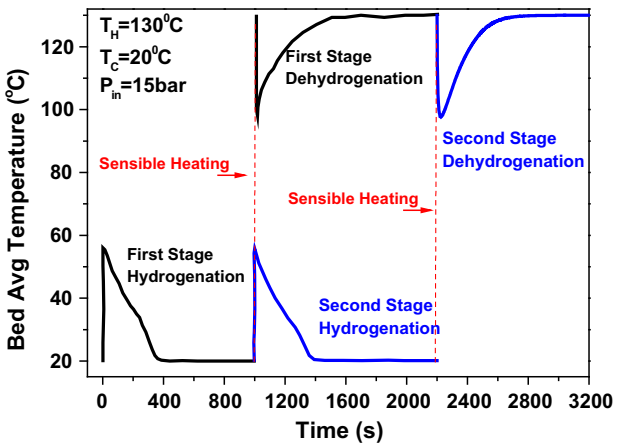

Fig. 13 Bed average temperature evolution for a complete hydrogen compression cycle

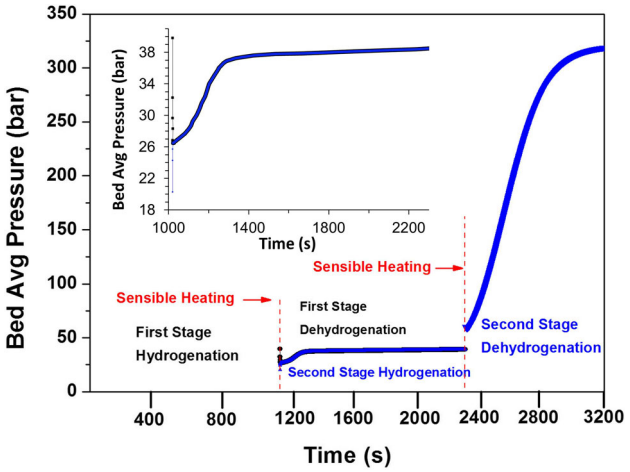

Fig. 14 Bed average pressure evolution for a complete hydrogen compression cycle

Fig. 15 HYMEHC-10 proof-of-concept compressor at HyNor Lillestrøm

during the hydrogenation process of the first stage, the hydrogen pressure within the reactor drops during the formation of the MH. At the beginning of the coupling, there is a maximum pressure difference between the two reactors of 20 bar. During the initial coupling, this pressure difference gets equalized, resulting in the pressure of stage 1 decreasing sharply from 40 bar and the pressure of stage 2 increasing rapidly from 20 bar. After the pressure equalizes across both reactors, the continuation of the coupling process results in a gradual increase in pressure until it reaches the equilibrium of the driving potential between the two reactors. The inset picture in Fig. 14 is of the coupled stages 1 and 2 reactors and illustrates the relatively fast kinetics of the two systems. At the end of the compression, the simulated system achieves a pressure of 325 bar resulting in a pressure ratio of 22:1.

4 Recent developments of industrial-scale MH hydrogen compressors

4.1 HYMEHC-5 and HYMEHC-10: the thermal hydrogen compressors by HYSTORSYS

Two full-scale proof-of-concept compressor systems have been constructed: one HYMEHC-10 (10 Nm^3/h thermal hydrogen compressor) and one HYMEHC-5 (5 Nm^3/h). The compressor systems are CE-marked and constructed for operation in Ex Zone 2 (according to IEC 60079-10-1, standard covering hazardous area classification for gases).

The HYMEHC-10 proof-of-concept thermal hydrogen compressor was developed and delivered to the HyNor Lillestrøm refuelling station located in Akershus Energy Park about 25 km northeast of Oslo as a part of the user-driven innovation project HyNor Lillestrøm founded by the Research Council of Norway, Akershus County Council, Transnova, Innovation Norway and Akershus Energy (www.hynor-lillestrom.no). In addition to being a refuelling station for hydrogen vehicles, HyNor Lillestrøm is a research and demonstration center for new hydrogen technologies.

The HYMEHC-10 unit shown in Fig. 15 was installed at HyNor Lillestrøm as a continuously operated compressor system increasing the pressure from 10 bar up to 200 bar at a throughput rate of 10 Nm^3/h.

This MH-based hydrogen compressor consists of three high-pressure steel vessels for each of the two stages. Each of the six vessels contains about 34 kg of MH material. An AB_5 alloy ($La_{1-x}Ce_xNi_5$) is used for the first compression stage from 10 to 50 bar, while an AB_2 alloy (Ti, Zr-based) is used for the second stage from 50 to 200 bar. The MH system operates with thermal cycles between 20 and 150 °C and requires only a small amount of electricity to power valves and other small pieces of auxiliary equipment.

An electrical external oil heater with a maximum capacity of 27 kW is installed to emulate the "industrial process heat," and the heat transfer to the MH compressor is facilitated by a heating oil loop using the commercially available oil THERMINOL®LT.

Thermal management of the compressor is based on two pressurized closed oil loops. Each of the six MH vessels is equipped with two three-way valves selecting the hot or the cold oil according to the thermal sequence diagram making only the compartment of the compressor vessels common for the two oil loops. Circulation of the oil is provided by means of two high-temperature circulation pumps. The flow of hydrogen is controlled by means of pneumatic shut-off valves. Each of the six pressure vessels is equipped with a pressure sensor and a temperature sensor continuously probing the "state" of each vessel. In addition, safety relief

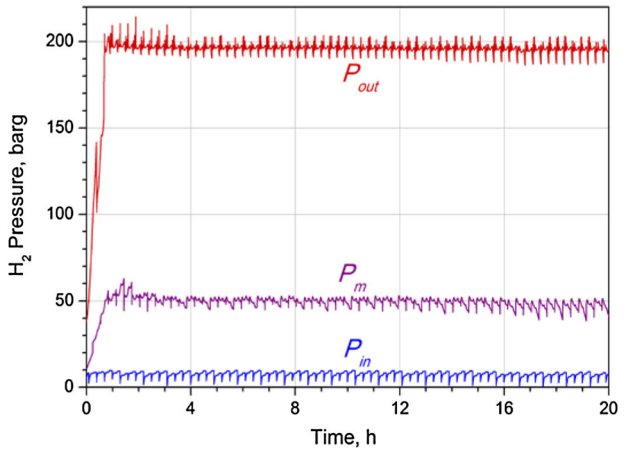

Fig. 16 Hydrogen pressures in HYMEHC-10 compressor: P_{in}—inlet pressure, P_m—intermediate pressure after first stage and P_{out}—outlet pressure after second stage

valves (burst pressure 250 bar) are implemented for each unit as well as at the compressor input/output.

The commissioning of the HYMEHC-10 at the HyNor Lillestrøm refuelling station started in May 2013. This system has been successfully tested and put into operation. Up to now HYMEHC-10 has been operated for about 3500 h, including a near-month operation in nonstop regime. The only maintenance during operating period was a replacement of a shut-off valve on hydrogen line (due to internal leakage), after about 2000 operation hours. Figure 16 shows hydrogen pressures at different stages of hydrogen compression during operation of HYMEHC-10 (oil temperatures are ~24 °C for cold loop and ~120 °C for hot loop).

The HYMEHC-5 proof-of-concept system was developed as part of the Eurostars project HYPROCOM that was carried out in collaboration with the Dutch reformer company HyGear (www.hygear.nl) and the industrial gas company Air Products (www.airproducts.com). The two-stage compressor has been constructed for continuous operation increasing the pressure from approximately 5 bar up to 230 bar (burst pressure for safety valves 250 bar) at a throughput rate of 5 Nm^3/h exploiting thermal energy of maximum 150 °C.

In general, the configuration and the instrumentation of the "HYPROCOM" HYMEHC-5 compressor are similar to those of the HYMEHC-10 described above. The main deviations compared to the HYMEHC-10 system are: (a) the lower hydrogen throughput rate, (b) the lower input pressure level/higher output pressure level and (c) the thermal integration with respect to the steam methane reformer (SMR) from HyGear.

The HYMEHC-5 was put into operation at the test site of NEL Hydrogen (Notodden, Norway) for internal R&D, making HYSTORSYS ready for deliveries of thermal

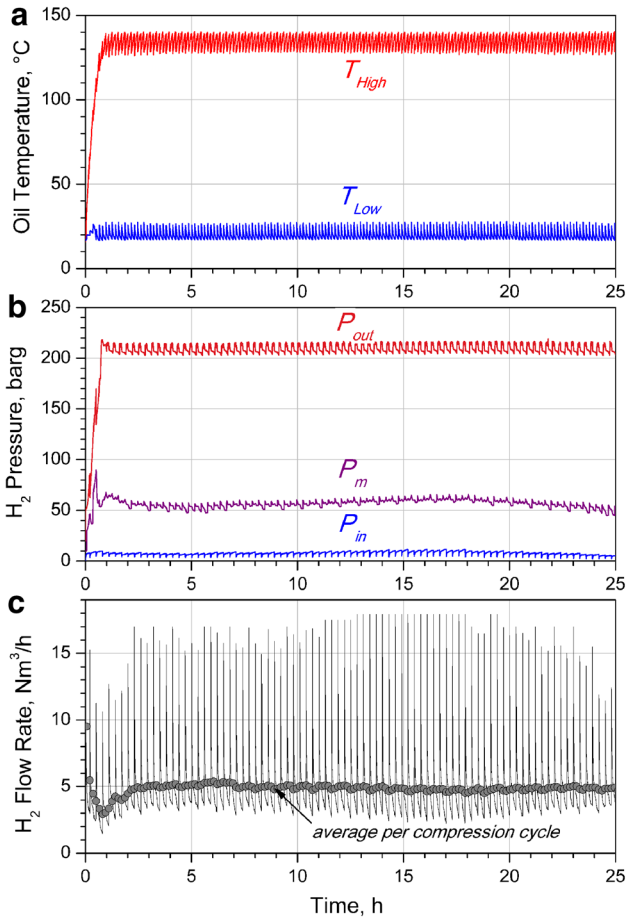

Fig. 17 Operating characteristics of HYMEHC-5 compressor: *a* temperatures of heat transfer fluid (Duratherm 450) in cold T_{Low} and hot T_{High} oil loops; *b* hydrogen pressures: inlet P_{in}, intermediate P_m and outlet P_{out}; and *c* hydrogen throughput rate

hydrogen compressor systems. The results of a continuous 25-h test operation of HYMEHC-5 at an upper temperature of 140 °C are shown in Fig. 17.

4.2 MH hydrogen compressor by SAIAMC/UWC (3–200 bar 5 Nm^3/h H_2)

A compressor was built by SAIAMC/UWC for the industrial customer, Eskom Holdings Ltd. (South Africa) for capturing low-pressure H_2 ($P_L \sim 3$ bar) delivered from PSA purification system and delivering the gas into standard gas cylinders at the pressure $P_H = 200$ bar. The available services necessary for the H_2 compression include low-grade steam ($T_H = 130$–150 °C) and circulating cooling water ($T_L = 20$–25 °C).

Preliminary analysis showed that the specified pressure–temperature requirements can be met using three-stage compressor layout. Figure 18 presents PCT characteristics of MH materials selected for the stages 1 (a; $LaNi_{4.9}Sn_{0.1}$),

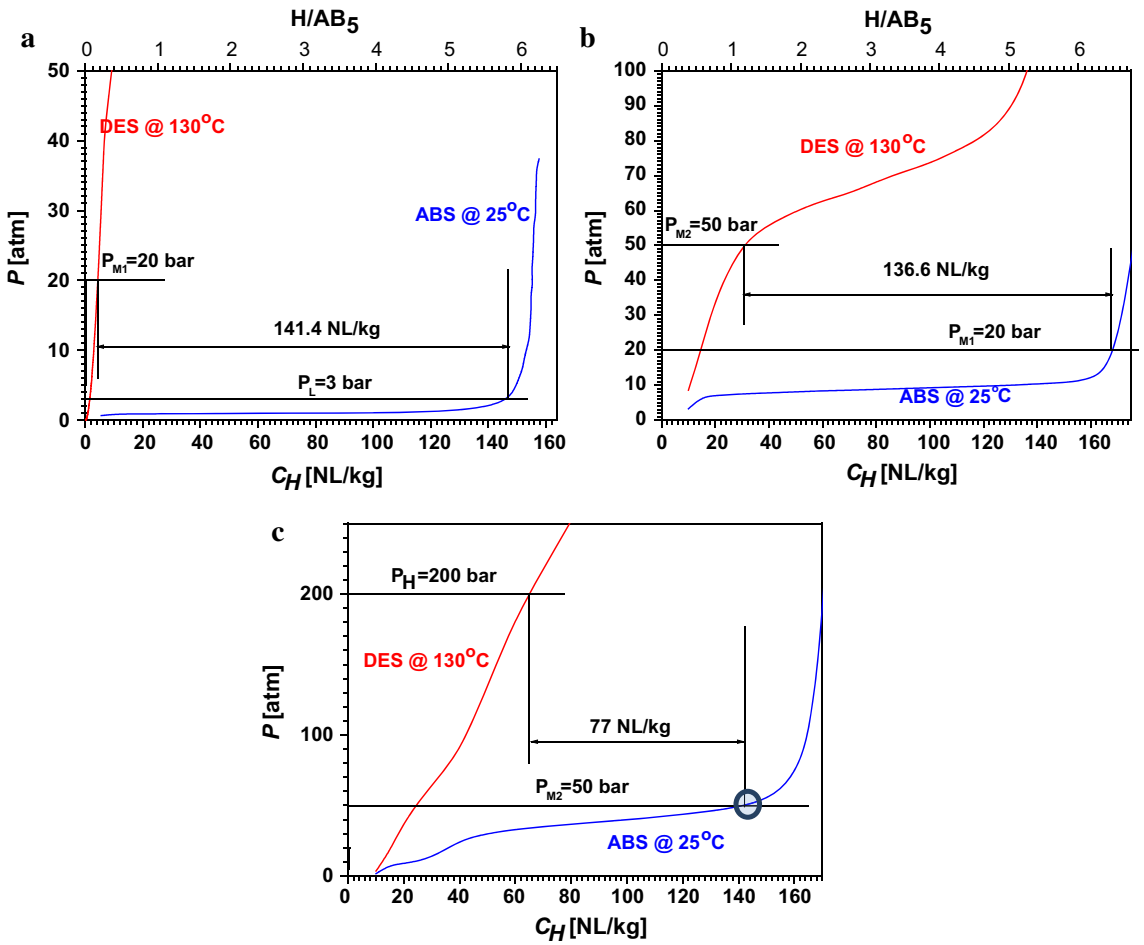

Fig. 18 PCT characteristics of the $LaNi_{4.9}Sn_{0.1}$ (**a**), $La_{0.8}Ce_{0.2}Ni_5$ (**b**) and 90 wt% C14-$Ti_{0.65}Zr_{0.35}(Mn,Cr,Fe,Ni)_2$ + 10 wt% $La_{0.8}Ce_{0.2}Ni_5$ (**c**) used in the H_2 compressor

2 (b; $La_{0.8}Ce_{0.2}Ni_5$) and 3 (c; C14-$Ti_{0.65}Zr_{0.35}$(-Mn,Cr,Fe,Ni)$_2$ with the additive of 10 wt% of $La_{0.8}Ce_{0.2}$-Ni_5 to facilitate the activation).

As shown in Fig. 18, the cycle productivity of the three-stage H_2 compression is mainly determined by hydrogen absorption/desorption in the AB_2-type material on stage 3 (c). In turn, at the given $T_L = 25$ °C, hydrogen concentration achieved in this material (circled area in Fig. 18c) is strongly dependent on the intermediate pressure, P_{M2}, determined by PCT performance of the second-stage material at $T = T_H$ (Fig. 18b). The reduction of P_{M2} from 50 ($La_{0.8}Ce_{0.2}Ni_5$) to 40 atm. ($La_{0.85}Ce_{0.15}Ni_5$) results in the drop of the cycle productivity in 1.7 times, from 77 to 45 NL/kg.

General views of the compressor are shown in Fig. 19. Apart from MH materials used for stages 1–3 (see above), the compressor has a number of original layout features, according to the engineering solution recently patented by UWC [26]. The main layout features aimed at the maximizing of the throughout capacity include:

1. Special gas piping allowing to apply different time setpoints for the heating and cooling which are optimal for the selected MH materials and containers.
2. Variation in the size of MH containers for stages 1, 2 and 3 allowing to increase pressure driving forces (P_{M1}, P_{M2}) in between the stages.
3. Hydrogen purification option, by partial release of contaminated H_2 from the stage 1 MH containers at the beginning of the heating/H_2 desorption.
4. Optimization of the layout of the MH container allowing to improve its heat transfer performances.
5. Optimization of heating/cooling piping diagram toward the increase in the heating/cooling efficiency and reduction in consumption of steam and water. In particular, usage of steam traps allowed us to significantly improve the heating efficiency above 100 °C and to achieve the steam consumption below 30 kg/h during the operation.

Hydrogen compression is provided by 12 MH containers assembled in two compression modules. Each module

comprises six MH containers (by two for each stage) which can be heated or cooled simultaneously, to provide higher pressure H_2 desorption and lower pressure H_2 absorption, respectively. The heating and cooling times can be set separately within the limits 15–45 min. The amount of the MH material in one container varies from 17 kg (stage 1) down to 12.5 kg (stage 3) according to the feature (2) listed above. The operation of the compressor is provided via a program logic controller (PLC), by the periodic opening and closing solenoid valves in the gas (stage 1 only) and steam/water piping circuits. Switching of high-pressure gas flows (stages 2–3) is provided automatically by a corresponding check valve arrangement.

Fig. 19 Front (*top*) and side (*bottom*) views of the MH compressor without sidewalls. The unit dimensions (mm) are: 2465 (L) × 1350 (W) × 1325 (H)

The compressor is able to compress hydrogen from 3 to 200 bar with average throughout capacity about 5 Nm^3/h using direct steam heating ($T_H = 130$ °C) and water cooling ($T_L = 25$ °C) to drive the H_2 compression. It was shown that the operating pressure range can be as wide as 1–240 bar at the same heating/cooling conditions, but in this case the throughout capacity significantly drops.

5 Summary, concluding remarks and future prospects

The main challenges in the development of the MH compressors include achievement of the necessary compression ratios within the available operation temperature range, as well as increase in the throughout capacity/productivity, cycle lifetime and improvement of the energy efficiency. These problems, being particularly critical for the industrial-scale multistage MH compressors, are addressed by (1) proper selection and development of the MH alloys; (2) improvement of the dynamic performances of the MH

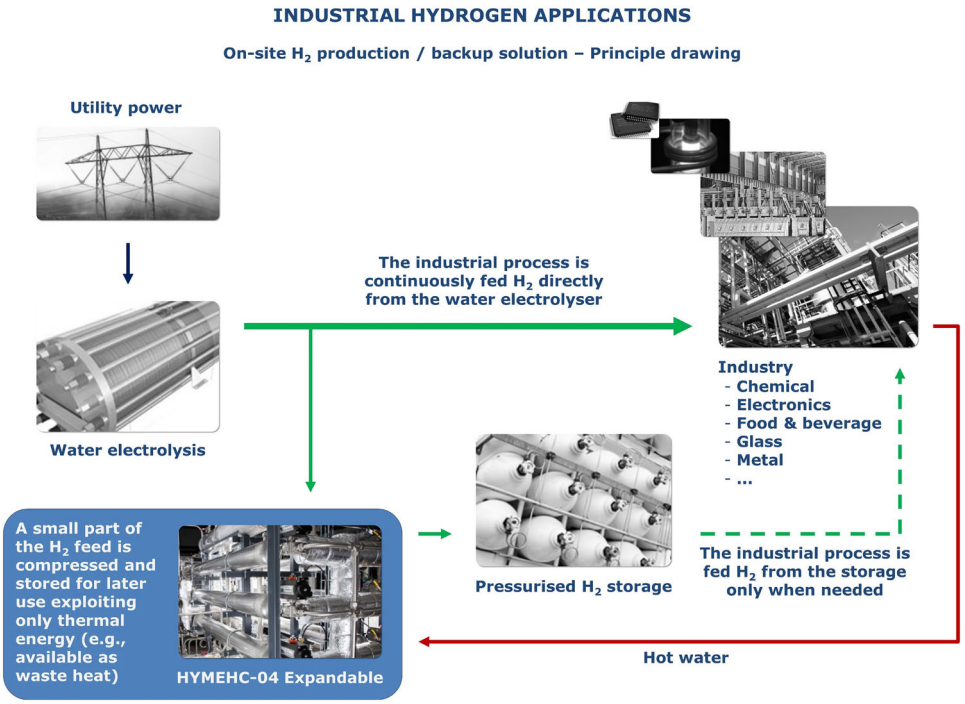

Fig. 20 Conceptual configuration for an on-site hydrogen production/backup solution to support industrial applications based on thermal hydrogen compression

containers; and (3) optimization of the overall system layout.

As mentioned, several research teams continue further investigations of the AB_2 alloys [2, 3, 27, 28] and AB_5 alloys [4, 5, 29–33]. These two groups of materials offer considerable potential possibilities for the optimization in both the alloys composition and in the technologies of their processing allowing to reach the desired performance levels.

The improvement of the dynamic performances of MH containers for H_2 compressors, as well as the whole system optimization, implies a precise modelling of the heat and mass transfer in the MH beds coupled in the multistage layouts. The increase in the modelling accuracy is very important and can be achieved, first of all, by the appropriate description of the PCT relationships in the metal–hydrogen systems. Based on the results of the modelling, advanced engineering solutions of both system components and general layout features may be drawn resulting in the solution of the problems specified above.

In general, the MH compressors can serve a number of markets such as traditional industry, renewable energy, emergency power, hydrogen fuel infrastructure. While some of these markets are still small but are emerging, hydrogen can be readily used in a number of industrial processes already today. Importantly, many industrial chemical processes generate large amounts of the waste heat that can be fed back to a MH compressor compressing hydrogen *for free*. Thus, we observe a good match between the traditional industry and thermally driven MH hydrogen compressors.

An overview conceptual drawing of an on-site hydrogen production/backup solution suggested by HYSTORSYS AS for industrial applications is shown in Fig. 20 [34]. Here, the industrial process continuously fed hydrogen from the on-site hydrogen generator (water electrolyzer or reformer unit), while occasionally a small part of the hydrogen feed is compressed and stored for later use exploiting only thermal energy—e.g., waste heat from the industrial process. The purpose of the hydrogen backup system (comprising the compressor and the storage) is to provide hydrogen for the industrial process whenever the direct hydrogen supply line is down (e.g., for hydrogen generator maintenance, utility power interrupt or other sort of failures). The size of such a hydrogen backup storage might very much vary from application to application. However, since the main supply line only will be down occasionally and the interference with the continuous hydrogen feed should be at a minimum, usually a small to moderate compressor capacity would need to be installed in order to top off the backup storage.

Figure 21 presents an example of this approach recently implemented by SAIAMC/UWC for Impala Platinum Ltd. in South Africa [35]. The MH compressor is integrated in hydrogen refuelling station (dispensing H_2 pressure up to 185 bar) for the refuelling of fuel cell forklifts. The dispensing is carried out from a buffer, standard cylinder pack (900 l in the inner volume, H_2 pressure 200 bar), while the high pressure in the buffer is maintained by MH compressor which is fed from H_2 pipeline consuming steam and cooling water available at the customer's site.

It appears to be very promising to use MH compressors for the industrial customers having in their possession low-pressure hydrogen supplied by a pipeline. As the cost of the pipeline hydrogen is much lower than the cost of compressed H_2 supplied in gas cylinders, the use of the MH compression is becoming a significant economic driver for the industrial-scale implementation of the MH compression technology. Even prototype MH compressors require only reasonable investments while keeping the low operation costs [1] in cases where instead of utilizing expensive

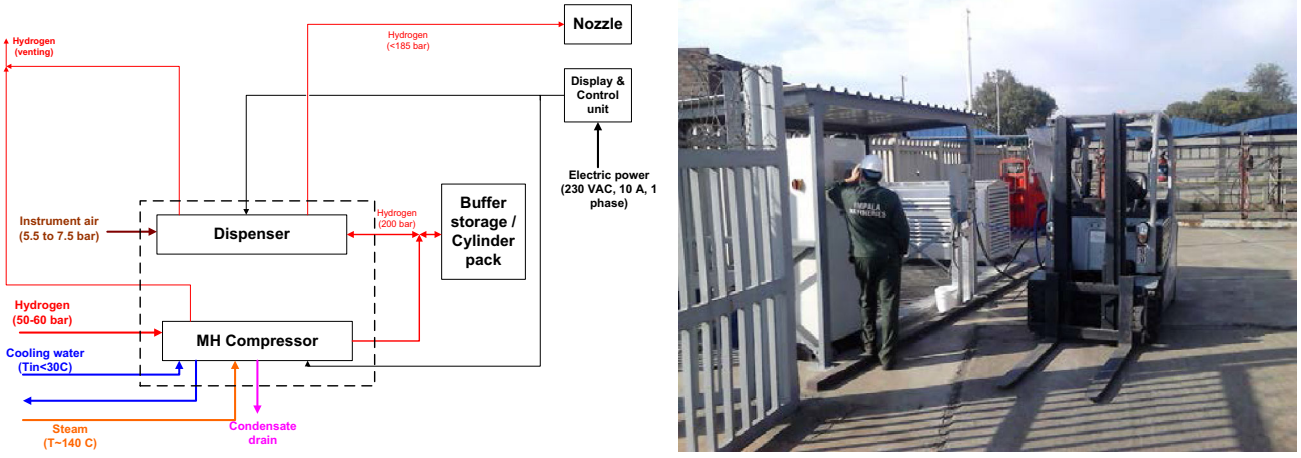

Fig. 21 Simplified layout (*left*) and general view (*right*) of hydrogen refuelling station with MH compressor developed by SAIAMC/UWC for Impala Platinum Ltd. (South Africa)

electric power, the services already existing in the customer's infrastructure (low-grade steam and circulating cooling water) can be utilized to offer economically efficient H_2 compression.

Acknowledgments This work is a part of the activities within IEA Task 32 Hydrogen Based Energy Storage. We are grateful for the task coordinator Dr. Michael Hirscher and all the experts from the Task 32 for the fruitful collaboration. Volodymyr A. Yartys acknowledges the support from the Research Council of Norway (Project 191106 "Thermally Driven systems for Storage, Compression and Supply of Hydrogen Gas") and Nordic Energy Research (Project NORSTORE). Development and characterization of MH materials for hydrogen compression was done via Program of Research Cooperation between Norway and South Africa funded by Research Council of Norway and NRF in South Africa (Project No. 180344 was coordinated by V.A. Yartys and M.V. Lototskyy). Mykhaylo Lototskyy and Vladimir Linkov acknowledge the support of Eskom Holdings Ltd. and Impala Platinum Ltd. (both from South Africa) for the funding of the developments of MH hydrogen compressors at South African Institute for Advanced Materials Chemistry. Furthermore, ML and VL acknowledge the support from the Department of Science and Technology (DST) in South Africa via Hydrogen South Africa National Flagship Hydrogen and Fuel Cell Programme (HySA; Project KP3-S02). David Grant, Alastair Stuart would like to thank the Engineering and Physical Science Research Council for funding under EP/K021117/1 and Evangelos Gkanas, Kandavel Manickam and Gavin Walker (University of Nottingham) for their valuable support. HYSTORSYS AS would like to acknowledge the support and dedicated contribution from the Eurostars-programme and the HYPROCOM-partners HyGear B.V. and Air Products and Chemicals, Inc., Hynor Lillestrøm AS for hosting the compressor test site and managing the HyNor-project, the founding bodies of the HyNor Lillestrøm-project being the Research Council of Norway, Akershus County Council, Transnova, Akershus Energy and Innovation Norway, and last but not least—Norsk Innovasjonskapital III AS (NIK III) for their committed financing of the company. Robert C. Bowman, Jr. thanks the Fuel Cell Technology Office of the U.S. Department of Energy, Office of Energy Efficiency and Renewable Energy for their support of his work at the Oak Ridge National Laboratory. This manuscript has been authored by UT-Battelle, LLC, under Contract No. DE-AC05-00OR22725 with the U.S. Department of Energy. The United States Government retains and the publisher, by accepting the article for publication, acknowledges that the United States Government retains a non-exclusive, paid-up, irrevocable, world wide license to publish or reproduce the published form of this manuscript, or allow others to do so, for United States Government purposes. VAY and ML appreciate help from Latchezar Bozoukov (LabTech Int. Co. Ltd.), Dyre Rostald (Raufoss Fuel Systems ASA), Prof. Jan Ketil Sollberg (Norwegian University of Science and Technology), as well as Jan Petter Maehlen, Nils Jorgen Svensen and Kristin Wickstrøm (Institute for Energy Technology) received at various stages of the work on the metal hydride compression at Institute for Energy Technology.

References

1. M.V. Lototskyy, V.A. Yartys, B.G. Pollet, R.C. Bowman Jr, Metal hydride hydrogen compressors: a review. Int. J. Hydrog. Energy **39**, 5818–5851 (2014)
2. E.D. Koultoukis, S.S. Makridis, E. Pavlidou, P. de Rango, A.K. Stubos, Investigation of $ZrFe_2$-type materials for metal hydride hydrogen compressor systems by substituting Fe with Cr or V. Int. J. Hydrog. Energy **39**, 21380–21385 (2014)
3. L. Pickering, D. Reed, A.I. Bevan, D. Book, Ti–V–Mn based metal hydrides for hydrogen compression applications. J. Alloys Compd. **645**, S400–S403 (2015)
4. S.A. Obregón, M.R. Esquivel, A quantitative analysis of the hydrogen sorption isotherms of $MmNi_{4.25}Al_{0.75}$. Proc. Mater. Sci. **8**, 752–759 (2015)
5. S.P. Malyshenko, S.V. Mitrokhin, I.A. Romanov, Effects of scaling in metal hydride materials for hydrogen storage and compression. J. Alloys Compd. **645**, S84–S88 (2015)
6. B. Satya Sekhar, P. Muthukumar, Development of double-stage metal hydride-based hydrogen compressor for heat transformer application. J. Energy Eng. **141**(4), 04014049 (2014). doi:10.1061/(ASCE)EY.1943-7897.0000246
7. E.I. Gkanas, D.M. Grant, A.D. Stuart, C.N. Eastwick, D. Book, S. Nayebossadri, L. Pickering, G.S. Walker, Numerical study on a two-stage metal hydride hydrogen compression system. J. Alloys Compd. **645**, S18–S22 (2015)
8. M.M.H. Bhuiya, C.Y. Lee, T. Hwang, S. Munira, R. Hopkins, H. Yoon, S.H. Park, K.J. Kim, Experimentally tuned dual stage hydrogen compressor for improved compression ratio. Int. J. Hydrog. Energy **39**, 12924–12933 (2014)
9. Y.K. Baichtok, A.K. Avetisov, Y.M. Baranov, R.G. Telyashev, V.Z. Mordkovich, S.V. Suvorkin, A.N. Obryvalina, N.V.Dudakova, G.V. Kosarev, N.A.Kostikov. Housing-tubular module of hydride thermal sorption hydrogen separator–compressor. Patent application US 2014/0311348 A1, 23.10.2014
10. M.M.H. Bhuiya, A. Kumar, K.J. Kim, Metal hydrides in engineering systems, processes, and devices: a review of non-storage applications. Int. J. Hydrog. Energy **40**, 2231–2247 (2015)
11. B.R.S. Hansen, K.T. Møller, M. Paskevicius, A.C. Dippel, P. Walter, C.J. Webb, C. Pistidda, N. Bergemann, M. Dornheim, T. Klassen, J.E. Jørgensen, T.R. Jensen, In situ X-ray diffraction environments for high-pressure reactions. J. Appl. Cryst. **48**, 1234–1241 (2015)
12. M.M.H. Bhuiya, Design and analysis of hydrogen powered actuator integrating metal hydride storage system. Ph.D. Thesis, University of Nevada, Las Vegas, 2014. Downloaded from Digital Scholarship@UNLV. http://digitalscholarship.unlv.edu/thesesdissertations
13. M.V. Lototsky, V.A. Yartys, V.S. Marinin, N.M. Lototsky, Modelling of phase equilibria in metal–hydrogen systems. J. Alloys Compd. **356–357**, 27–31 (2003)
14. M. Lototskyy, Y. Klochko, V. Linkov, P. Lawrie, B.G. Pollet, Thermally driven metal hydride hydrogen compressor for medium-scale applications. Energy Proc. **29**, 347–356 (2012)
15. H.A. Kierstead, A theory of multiplateau hydrogen absorption isotherms. J. Less-Common Met. **71**, 303–309 (1980)
16. R.H. Wiswall, J.J. Reilly, Method of storing hydrogen US patent 3516263 (1970)
17. A.N. Golubkov, S.K. Grishechkin, A.A. Yukhimchuk, System for investigation of hydrogen isotopes—solid body interaction at 500 MPa. Int. J. Hydrog. Energy **26**, 465–468 (2001)
18. Y.F. Shmal'ko, V.V. Solovey, M.V. Lototsky, E.V. Klochko, I.Y. Zavaliy, O.B. Ryabov, V.A. Yartys, Metal-hydride systems for processing hydrogen isotopes for power plants. Mater. Sci. **37**(5), 689–706 (2001)
19. M.V. Lototsky, A.F. Savenko, D.V. Schur, V.K. Pishuk, V.A. Yartys, A.P. Mukhachev, Metal hydride unit for hydrogen storage/compression, in *IX International Conference in Hydrogen Materials Science and Chemistry of Carbon Nanomaterials (ICHMS'2005)*, Sevastopol, Crimea, Ukraine, 05–11 September 2005, pp. 822–825

20. G. Sandrock, A panoramic overview of hydrogen storage alloys from a gas reaction point of view. J Alloys Compd. **293–295**, 877–888 (1999)
21. B.A. Kolachev, R.E. Shanin, A.A. Il'in, *Hydrogen Storage Alloys/Reference Book* (Metallurgy Publications, Moscow, 1995). **(in Russian)**
22. K. Nasako, Y. Ito, N. Hiro, M. Osumi, Stress on a reaction vessel by the swelling of a hydrogen absorbing alloy. J. Alloys Compd. **264**, 271–276 (1998)
23. V. Yartys, M. Lototsky, Y. Tranøy, R. Glöckner, *Hydrogen Storage and Applications: An Overview*. Report IFE/KR/F-2003/
24. P. Muthukumar, A. Singhal, G.K. Bansal, Thermal modeling and performance analysis of industrial-scale metal hydride based hydrogen storage container. Int. J. Hydrog. Energy **37**, 14351–14364 (2012)
25. T. Nashizaki, K. Miyamoto, K. Yoshida, Coefficients of performance of hydride heat pumps. J. Less Common Met. **89**, 559–566 (1983)
26. M.V. Lototskyy, D. Swanepoel, M.W. Davids, Y. Klochko, B.J. Bladergroen, V.M. Linkov. Multistage metal hydride hydrogen compressor. Patent application ZA 2015/01837, 18 Mar 2015
27. E.D. Koultoukis, S.S. Makridis, D. Fruchart, A.K. Stubos, Two-stage hydrogen compression using Zr-based metal hydrides. Solid State Phenom. **194**, 249–253 (2013)
28. E.D. Koultoukis, E.I. Gkanas, S.S. Makridis, C.N. Christodoulou, D. Fruchart, A.K. Stubos, High-temperature activated AB_2 nanopowders for metal hydride hydrogen compression. Int. J. Energy Res. **35**, 477–486 (2014)
29. B.A. Talaganis, M.R. Esquivel, G. Meyer, A two-stage hydrogen compressor based on (La, Ce, Nd, Pr)Ni5 intermetallics obtained by low energy mechanical alloying—low temperature annealing treatment. Int. J. Hydrog. Energy **34**, 2062–2068 (2009)
30. B.A. Talaganis, M.R. Esquivel, G. Meyer, Improvement of as-milled properties of mechanically alloyed $LaNi_5$ and application to hydrogen thermal compression. Int. J. Hydrog. Energy **36**, 11961–11968 (2011)
31. S.A. Obregon, J.J. Andrade-Gamboa, M.R. Esquivel, Synthesis of Al-containing $MmNi_5$ by mechanical alloying: milling stages, structure parameters and thermal annealing. Int. J. Hydrog. Energy **37**, 14972–14977 (2012)
32. S.A. Obregon, M.R. Esquivel, Scheme of thermal compression of hydrogen (TCH) using $MmNi_{4.25}Al_{0.75}$ recovered with ethyl alcohol and handled under non protective atmospheres. Int. J. Hydrog. Energy **39**, 8577–8581 (2014)
33. M. Odysseos, P. De Rango, C.N. Christodoulou, E.K. Hlil, T. Steriotis, G. Karagiorgis, G. Charalambopoulou, T. Papapanagiotou, A. Ampoumogli, V. Psycharis, E. Koultoukis, D. Fruchart, A. Stubos, The effect of compositional changes on the structural and hydrogen storage properties of (La–Ce)Ni_5 type intermetallics towards compounds suitable for metal hydride hydrogen compression. J. Alloys Compd. **580**, S268–S270 (2013)
34. HYSTORSYS AS, HYMEHC-04 Expandable, data sheet, 2015
35. M.V. Lototskyy, I. Tolj, M.W. Davids, Y.V. Klochko, A. Parsons, D. Swanepoel, R. Ehlers, G. Louw, B. van der Westhuizen, F. Smith, B.G. Pollet, C. Sita, V. Linkov, Metal hydride hydrogen storage and supply systems for electric forklift with low-temperature proton exchange membrane fuel cell power module. Int. J. Hydrog. Energy (2016). http://dx.doi.org/10.1016/j.ijhydene.2016.01.148